Gyroscope technologies for space applications

M. N. Armenise, C. Ciminelli, F. De Leonardis, R. Diana, V. Passaro, F. Peluso

Optoelectronics Laboratory, Dipartimento di Elettrotecnica ed Elettronica, Politecnico di Bari
Via Orabona n.4, 70125 Bari, Italy, e-mail: **armenise@poliba.it**

Abstract

In this paper a review of the gyroscope technologies for space applications is reported. For each technological approach the principle of operation, advantages and disadvantages are discussed. Also, some future trends are predicted.

1. Introduction

Guidance, navigation and control systems both in aircrafts and spacecrafts require gyroscopes to maintain orientation in flight even in case of undesired interference. In particular, the measurement of the angular motion of a satellite in the space is essential for the control and stabilization of its attitude. Systems employing a gyroscope include the control and processing electronics to provide the most direct method for sensing inertial angular velocity.

Navigation systems, including also land transport vehicles, require gyroscopes with a sensitivity as low as 10-100°/s, attitude and heading reference systems in the airplanes use 1°/s gyroscopes, while precision inertial navigation systems [1], such us military airplanes and ships, spacecrafts and satellites, need a sensitivity value as high as 0.01-0.001°/s.

This paper presents a review of gyroscope devices [2]. The main technological categories are described in detail. For each of them, the operating principle, device structures, fabrication technology, specifications, open issues related to the design, packaging and interface electronics are discussed. A comparison among the performances allowed by the different technologies is also presented together with an indication of the future trends for the development of high – performance gyroscope, devoted to space applications.

2. Gyroscope technologies

The gyroscopes described in the following subsections are: fiber optic gyros, ring resonator gyros, micro-electro-mechanical-system gyros and micro- optical-electro-mechanical-system gyros.

2.1 Fiber-optic gyros

2.1.1 Interferometric fiber-optic gyros (IFOGs)

They were first proposed in '60s and developed rather slowly because appropriate laser sources were not available. IFOGs are based on the Sagnac effect [3]. In particular they are phase sensitive devices. Sagnac effect generates an optical phase difference, $\Delta\Phi_S$, between two counterpropagating waves in a rotating fiber coil (optical path) [3]:

$$\Delta\ddot{O}_S = S\grave{U} = \frac{4\eth RL}{\ddot{e}c}\grave{U} \qquad (1)$$

where S is the scale factor, Ω is the angular velocity around the rotation axis, R is the fiber coil radius, L is the optical path length, λ is the optical wavelength and c is the velocity of light in vacuum. The effect is non-reciprocal: the counterpropagating beams acquire Sagnac phase shift of opposite sign and different value. In a general formulation, the phase shift depends only on the light frequency ω and on the dot product of the equivalent area vector **A** of the average optical path and the rotation rate vector **W**:

$$\Delta\ddot{O}_S = \frac{4\grave{u}}{c^2}\mathbf{A}\grave{\mathbf{U}} \qquad (2)$$

As it is shown in the previous equations, the phase shift is an indirect measurement of the rotation rate Ω. Some design considerations can also be derived from Eqns (1) and (2). In fact, both longer and larger coils increase sensitivity (which is the capability of the output photocurrent to follow the variation of the input rate) because sensitivity is proportional both to diameter and total length of the optical path. However, it should be considered that larger coils are more sensitive to temperature variations and vibrations.

If P_D is the power that impinges on photodiode, expressed as

$$P_D = \frac{1}{2}P_0\left(1+\cos\ddot{A}\ddot{O}_S\right), \qquad (3)$$

the sensitivity is given by:

$$\frac{dP_D}{d\Omega} = -\frac{1}{2} P_0 sen\Delta\Phi_S \frac{4\pi LR}{\lambda c} \quad (4)$$

where P_0 is the input power. The maximum value is obtained for $\Delta\Phi_S = \pi/2$, i.e. where the fringe slope of the interferometer is at the maximum value. A further consideration is that sensitivity is also inversely proportional to wavelength, but increasing sensitivity by using shorter wavelength results also in a reduction of the radiation resistance of the optical fibres.

The uncertainty in the measurement (that is also the minimum detectable rotation rate) is $d(\Delta\Phi_S)$ = shot noise/fringe slope. The design of IFOG is, then, focused on reducing all noise sources below the photon noise at the detector.

Interferometric fiber-optic gyro can operate with two different configurations: open loop and closed loop. In the open loop configuration the information about the angular rate is obtained directly by the electrical signal at the output. In the closed loop a non-reciprocal phase shift is generated in the feedback loop to null the total phase shift. The applied opposite phase shift gives the information about the rotation rate.

Figure 1 represents an open loop configuration scheme and clarifies the principle of operation of this kind of sensor.

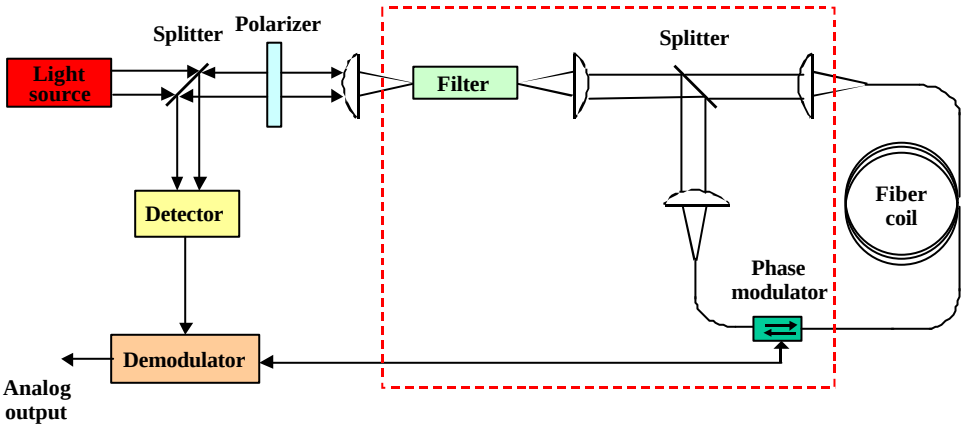

Fig. 1. Architecture of open loop IFOG

As in any interferometric device, the output signal is the result of the interference between two waves that, in this case, are counterpropagating in the optical fibre. This scheme is called “minimum configuration” which means it is able to guarantee the reciprocity of the system. To accurately measure the Sagnac effect and, then, increase the gyroscope quality, it is necessary to reduce any phase differences different from that induced by the rotation. Thus, reciprocity is the fundamental

requirement for IFOG. The dashed block shows the components that usually are integrated on a single chip.

The source beam is coupled into an optical path. The light pass through an optical system composed by a filter and polarizers to select and guarantee the presence of just one mode in the structure. This is because each mode in the structure has an independent light path that can experience environmental perturbations, different from those relevant to another mode. If the clockwise (CW) and counterclockwise (CCW) beams correspond to different modes, reciprocity is not achieved. Also, the fiber in the coil is required to be polarization-maintaining to ensure that just one mode does exist in the structure. The second splitter is used to create, in the fiber, two counterpropagating waves that sense Sagnac effect. After the coil the two beams recombine into the interferometer, the light passes again through the polarization control system and is directed on the photodetector by the second splitter. The phase modulator is used to apply a dynamic phase bias [4] generated by a sinusoidal wave to the light path, thus increasing sensitivity. If the modulation frequency f_m is sufficiently high, the electronic noise is avoided. The signal at the output of the photodiode is demodulated and processed for producing an output corresponding to the magnitude and sense of the rotation.

The optical source used in an IFOG is a broadband multi-mode laser or a superluminescent source to reduce the gyro signal noise due to coherent Rayleigh scattering generated by the counterpropating beams [5]. Either semiconductor or doped fiber sources can be used, depending on the desired performance of the gyro.

Main advantages for the open loop scheme are: low-price due to the use of a small number of commercial components, both electronic and optics, good sensitivity, and long lifetime and high reliability. Furthermore it has a low power consumption due to the low power consumption of the electronics and low driving power required by the laser; it is also insensitive to shocks and vibrations due to the interferometric structure, and insensitive to gravity or acceleration because it is not based on inertial forces and it doesn't need any tight control of the fibre length with respect to a frequency sensitive device. Disadvantages are the use of a very long single mode fibre to increase sensitivity, the drift caused by the analog components and the influence of temperature and environmental conditions.

To overcome the main issues of the open loop configuration, a closed loop device can be used. Very high performance has been obtained [6] with respect to open loop devices. The general scheme of a closed loop IFOG is in figure 2.

In the scheme the demodulator output passes through a servo amplifier which drives a phase transducer placed in the interferometer. The total phase shift becomes equal to zero because the phase

transducer introduces a non reciprocal phase shift that is equal, but opposite in sign, to that generated by the Sagnac effect when the device rotates. The output of the system is then the output of the phase transducer. Advantages of this scheme with respect to the open loop one is insensitivity to light source intensity variations and to gain variations of single component, because the system is always operated at zero. This implies a very small drift 0.001 to 0.01°/h. The output linearity and stability depend only on the phase transducer.

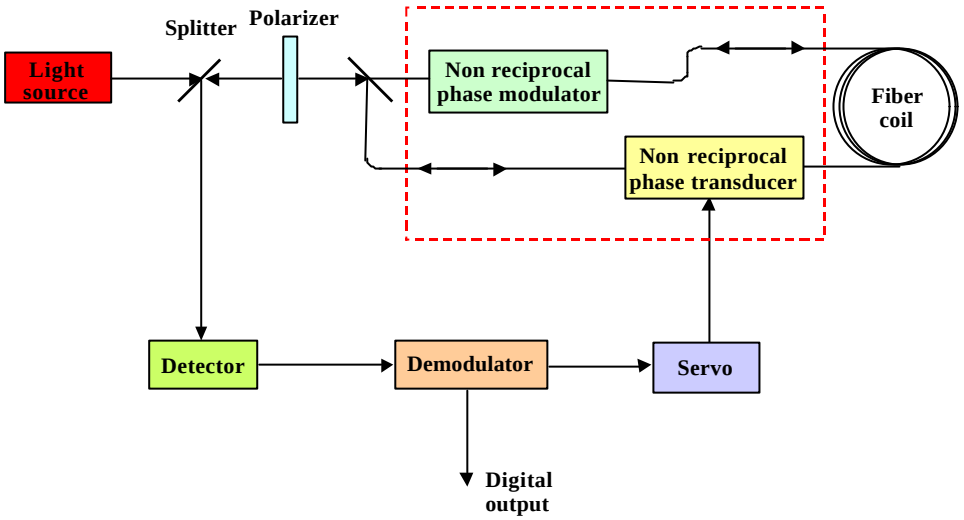

Fig. 2. Architecture of closed loop IFOG

Typical performance reported [7-16] for the interferometric fiber-optic gyros are an input range of ±100 °/s, a drift (bias) between 0.001 and 0.2 °/ h with a drift stability ranging from 0.0005 and 0.01 °/ h. Random walk is in the range $0.004 \div 0.04$ °/$\sqrt{h}$ and the bandwidth changes from 20 to 100 Hz.

IFOGs have long been used for terrestrial applications. These gyro systems are extremely robust and they are commercially available for use in space due to their relatively high reliability and cost effectiveness.

2.2 Resonant fiber-optic gyros (RFOGs)

A resonant fiber optic gyro configuration is illustrated in figure 3.

It is a frequency sensitive device in which the Sagnac effect generates a frequency difference between two resonant beams in the ring fiber cavity, locked to the resonant clockwise and counterclockwise frequencies. Resonance condition is $\beta_{\pm}L = 2m\pi$ that can be rewritten in terms of wavelength as $(2\pi/\lambda_{\pm})nL_{\pm} = 2\pi m$. From this last equation, $f_{\pm} = mc/nL_{\pm}$ can be derived, where L =

$2\pi R$. L_+ and L_- are the path lengths for clockwise (CW) and counter-clockwise (CCW) conterpropagating beams, respectively, and f_+ and f_- are the corresponding frequencies. When the device is rotated, these changes in length result in a change of the resonant frequencies in the cavity.

The output from a laser at frequency f_0 is split into two beams, each of them passing through an acoustooptic frequency shifter. The frequencies of the two beams are shifted by f_1 and f_2 to coincide with the CW and CCW resonant modes.

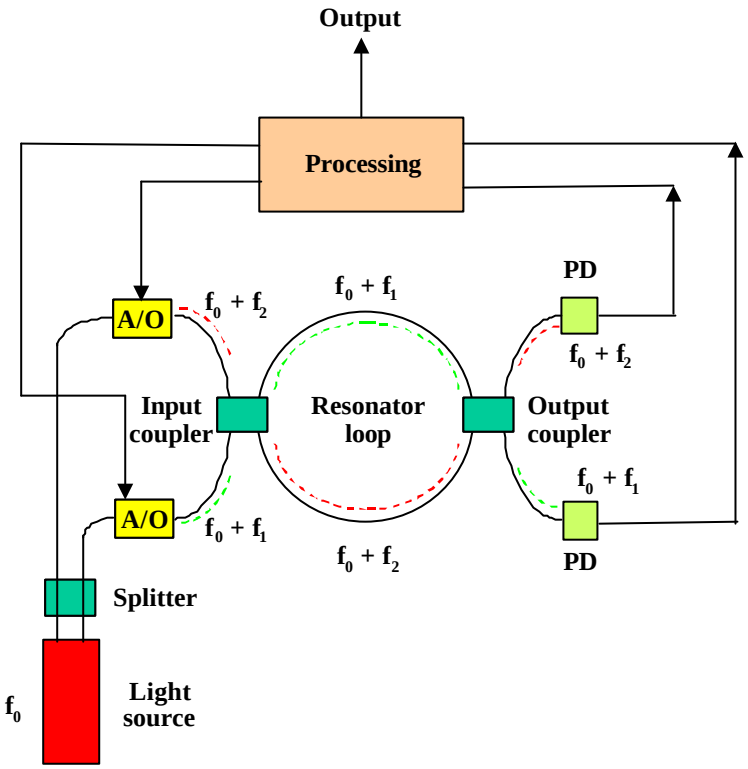

Fig. 3. Resonant fiber-optic gyro scheme

A fiber coupler is used to couple the beams into counterrotating waves in the fiber cavity. Without any rotation, the cavity resonant modes have the same frequency so, the initial frequency shift values for both CW and CCW beams are equal. A second fiber coupler is used to couple the counterrotating waves to the two photodetectors. The photodetector outputs are used to calculate feedback signals to drive the acoustooptic frequency shifters. If the two detectors reveal the maximum value of the expected power this means that the two input beams are perfectly locked to the resonance frequencies inside the cavity. If it doesn't happen, the processing unit caluculates the optimal frequency values to obtain the locking and calculate the signals to rearrange the shifters. The feedback loops lock

the frequencies $f_0 + f_1$ and $f_0 + f_2$ to the CW and CCW resonances of the fiber cavity. The frequency difference between the imposed frequency shifts is a meaurement of the rotation rate:

$$\Delta f = \frac{4A}{\lambda P}\Omega \tag{5}$$

where A is the area enclosed by the coil, λ is the wavelength of light, P is the perimeter of the fiber coil and Ω is the rotation rate.

The measurement uncertainty on the frequency-sensitive fiber devices is:

$$d\Omega = \frac{\lambda P}{4A}\frac{\sqrt{2}\Gamma}{SNR} \tag{6}$$

where Γ is the width of the resonant peaks of the fiber and SNR is the signal-to-noise ratio at the photodiode.

The main advantages of RFOG are high reliability and small amount of fiber with respect to the interferometric device due to the larger scale factor. Disadvantages are mainly represented by the need of a highly coherent laser source to increase sensitivity because, as it is shown in Eqn. (6), the measurement uncertainty is proportional to the linewidth of the resonant modes. The sensitivity can be increased by using some matching techniques between the frequency of optical beams and the resonant frequencies of the cavity, and low-loss components because an higher optical power results in a higher sensitivity.

No significant experimental results have been obtained so far.

2.2 Ring resonator gyros

They are based on the same principle of the resonant fiber-optic gyro seen in the previous subsection. Two main categories can be identified, both based on frequency shift (Sagnac effect) generated by the rotation: active ring resonator gyros and passive ring resonator gyros.

For a circular ring, the round trip path difference between CW and CCW counterrotating beams is $\Delta L = c\Delta t = 4\pi R^2\Omega / c$. At the same time, for a path length of L at λ, the resonance condition can be expressed as $m\lambda_\pm = L_\pm$, i.e. $\omega_\pm = mc/L_\pm$ (integer m). The frequency difference between the two CW and CCW beams is:

$$\Delta\omega = \omega_+ - \omega_- = mc\,\Delta L/L^2 \approx \omega\Delta L/L \tag{7}$$

The scale factor of the frequency sensitive devices is larger than that of the phase sensitive ones.

2.2.1 Active ring resonator gyros

In an active ring resonator gyro an active medium is introduced inside the ring cavity. The general scheme of the cavity, which includes a laser emitting on both sides and an optical path formed by mirrors is reported in figure 4.

These active sensors show a wide dynamic range (> 10^9) and a fast update rate. They are vibration insensitive and have a long and reliable lifetime (> 30,000 hours). Disadvantages are, mainly, a not high sensitivity and some performance limitations as null shift and lock-in effect.

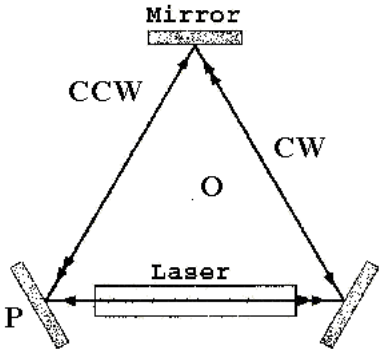

Fig. 4. Active ring resonator gyro scheme

The output characteristics of an active ring resonator gyro are reported in figure 5. The ideal behaviour of the gyro output is in figure 5a.

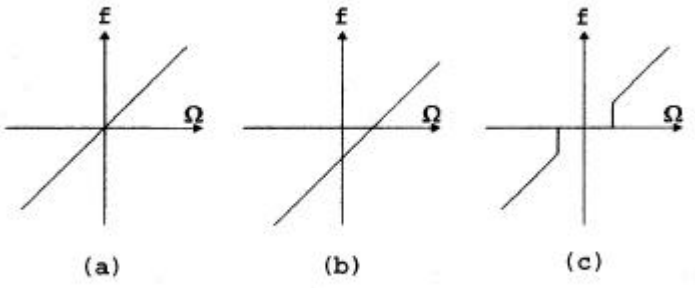

Fig. 5. Output characteristics of an active ring resonator gyro

In Fig. 5b one can observe that a non zero frequency difference (null shift) [17] can be obtained at zero input rate. This is due to the anisotropy of the cavity with respect to radiation travelling in the two directions. If repeatable it can be measured and compensated (constant bias of opposite value by means of a continuos rotation). Figure 5c describes the lock-in effect [17]: at very small rotation rates frequenc y difference is zero, defining a dead-band. It is mainly due to the weak coupling effects between independent counter-rotating beams. This effect results in a backscattering from one wave into the other one at the mirrors or inside the cavity. The problem is solved by using mechanical (optical) dithering [18] (alternating bias): the gyro is rotated in alternating way in one direction and in the opposite one.

It is possible to calculate the lock-in threshold and, hence, the minimum detectable rotation rate Ω_{th} when just the lock-in effect is taken into account:

$$\dot{U}_{th} = \frac{b}{S} = \frac{L}{2} \beta \quad (8)$$

where b is the backscattering coefficient.

Drift stability of 0.02 °/h, scale factor of 1.164.352 ps/rev with a stability equal to 20 ppm have been reported [19-21]. Random walk is 0.02 °/√h, operation temperature range is -54 to +85 °C and the power consumption 0.37 W at 5 Vdc. The gyro seems to be mainly devoted to tactical applications.

2.2.1.1 Integrated optic ring laser gyro

An example [22-23] of integrated optic ring laser gyro is reported in figure 6. The operating principle is again the frequency sensitivity due to Sagnac effect.

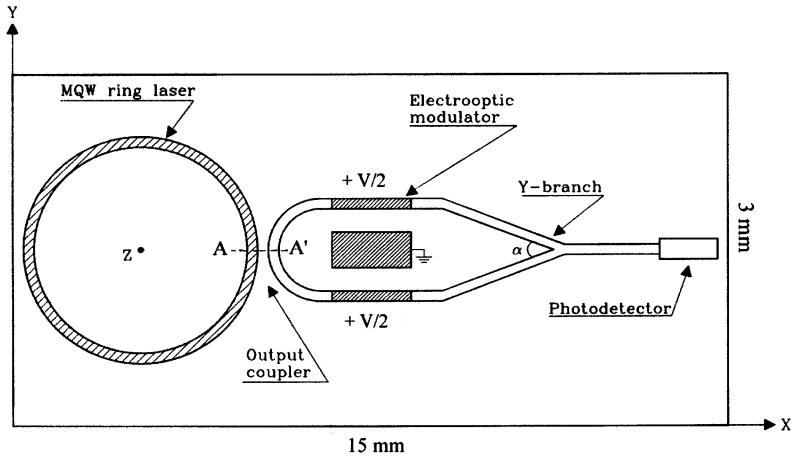

(a)

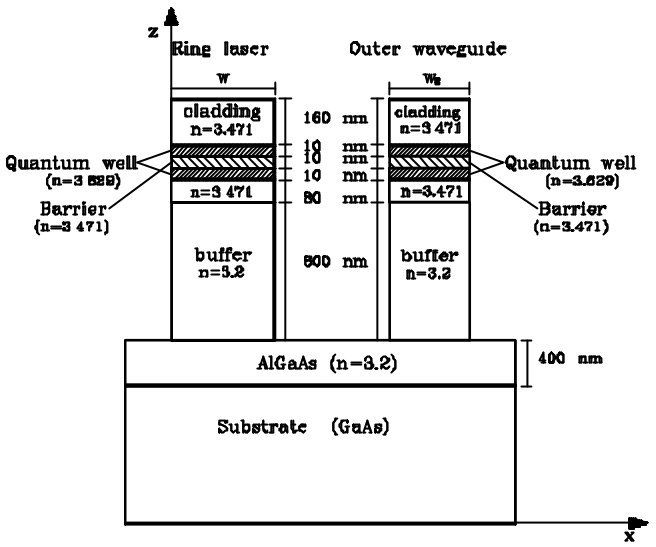

(b)

Fig. 6. Scheme of integrated optic ring laser gyro: a) sensor architecture; b) A-A' transverse section

The ring and the circular coupler are multiquantum well (MQW) structures in GaAs/GaAlAs. The beams generated inside the ring laser are coupled out by the coupler, pass through the two waveguides and are combined at the Y junction. An electrooptic modulator is used to induce a phase modulation mainly for two reasons: to erase any initial offset and to identify the direction of rotation through fast Fourier transform of the photocurrent. The presence of MQWs in the active region ensure a strong anisotropic optical gain, which is much greater for TE modes than for TM modes. So, the laser emits only TE modes and the sensor is polarization selective. Therefore, neither effects of birefringence and coupling between the two polarizations, nor polarization noise can be observed. The overall dimensions of the chip are 15 mm x 3 mm, ring radius is 1.5 mm and ring width is 0.3 μm.

Advantages of this approach are integration of different optical functions on a single chip of very small dimensions, reduction in size and mass, absence of any matching technique between the optical beam frequencies and the cavity resonant frequencies, high polarization selectivity, negligible curvature losses because of the strong optical field confinement due to the presence of the MQWs structure, high quality factor, good sensitivity and relatively low quantum limit. Quantum limit [17] is an intrinsic noise due to laser operation, in particular it is due to the spontaneous emission. It enlarges the beam linewidth increasing the measurement uncertainty and, then, reducing the sensitivity of the sensor. This kind of noise is related also to the sidewall roughness which is responsible for some backscattering effect inside the ring. It decreases when the effective ring radius increases and the

optical losses of the cavity decrease. Disadvantages for the integrated optic ring laser gyro are lock-in and possible mode competition, that is an effect due to the variation of the gain in the active medium for which bidirectionality of ring laser is lost. Main performance are quality factor of $2.24\ 10^6$, resolution of $3.5\ 10^{-6}$ °/s and power consumption of 1 W.

This gyro represents the most recent advance in the field, and it can be used mainly for spacecraft and satellite applications.

2.2.2 Passive ring resonator gyros

The second category of ring resonator gyros is the passive one. The main feature is that the source is external to the cavity as shown in figure 7.

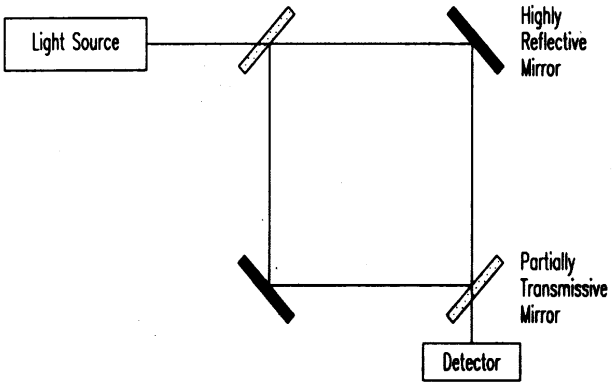

Fig. 7. Scheme of passive ring resonator gyro

As in the case of fiber ring resonator, light is split in two beams coupled into the cavity. At the output, the frequency difference between the beams carries the information about the rotation rate.

Advantages are a high sensitivity due to the absence of gain variations of the laser, low cost of fabrication, shock and vibration immunity due to the absence of moving parts, low power consumption for the small number of the components, high polarization selection in guided-wave structures that avoids polarization fluctuation induced noise and Kerr effect that are present in IFOG devices, high reliability. Moreover, passive structures solve problems of the active configuration such us lock-in effect and mode competition. Disadvantages are the need of low-loss waveguides and large ring radius to obtain high finesse and low quantum limit.

Two examples of passive ring resonator gyros are reported in the following. First configuration [24], reported in figure 8, is a silicon integrated optic waveguide chip.

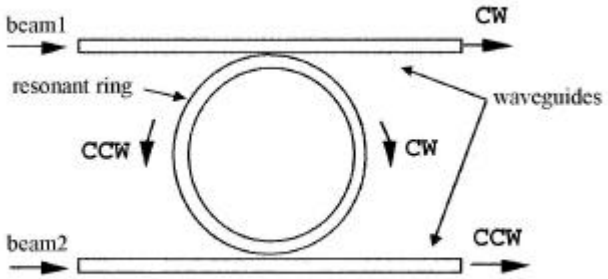

Fig. 8. Scheme of silicon integrated optic waveguide passive ring resonator gyro

A semiconductor laser source is split into two waveguides. The beams 1 and 2 produce the CCW and CW modes inside the ring. The information about rotation rate is in the phase difference between the output signals. Rate response have been obtained in the range of 1 to 200°/s [24].

In the scheme [25] reported in figure 9, a directional coupler, which launches light into the resonator, is composed of a Mach-Zehnder interferometer with a thermooptic phase shifter.

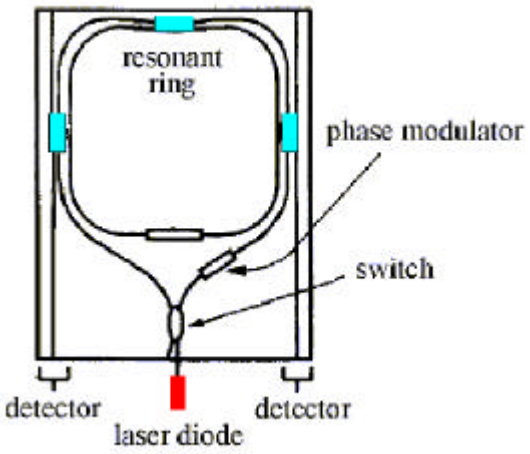

Fig. 9. Scheme of fully integrated resonant ring gyro

This approach represents a solution for strongly reducing the backscattering induced noise, which is the most serious noise factor in optical passive resonator gyros. The phase modulator induces a binary phase shift keying modulation (BPSK) on the carrier, putting the backscattered lightwave and the counter propagating signal out of the gyro bandwidth. However, it doesn't seem appropriate for space

applications. In fact, it has been proposed for substituting FOGs for car navigation, robotics and similar applications.

2.3 Micromachined-Electro-Mechanical-System (MEMS) gyros

MEMS gyroscopes make use of vibrating mechanical elements to sense rotation. They are fabricated by using the micromachining techniques in silicon or piezoelectric materials. In those gyroscopes a resonant primary excited mode contributes, together with Coriolis acceleration produced by the rotation, to a secondary resonant mode which gives the measure of the rotation.

The operating principle of vibrating gyros is the same for the different kinds of device. In particular, those gyros can be modeled by a mass-spring system as shown in Fig. 10.

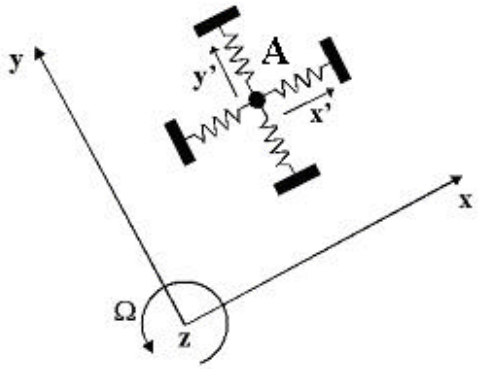

Fig. 10. Mass-spring system – vibrating MEMS gyroscope operating principle

The elementary sensing unit is represented by a particle A and the spring represents the elasticity of the particle supporting structure. The particle has two degrees of freedom; at any time instant its movement is defined by the displacements x' along x-axis e y' along y-axis. A rotation of the plane xy, that is the reference frame, around an orthogonal z-axis is characterized by an angular rate. To measure it, a vibration of the particle along x-axis must be first induced; the vibration amplitude has to be constant. This oscillation is indicated as the primary motion of the gyroscope or drive mode. The vibration is produced by a feedback control system, which excites the particle at its resonant frequency while maintaining the vibration amplitude at a set value.

When the gyroscope rotates, the particle experiences a Coriolis force, F_c, which has an amplitude proportional to the applied rotation rate Ω and its direction is, in the rotation frame, perpendicular to the primary motion direction:

$$F_c = 2mv \times \Omega \tag{9}$$

where m is the vibrating mass and v is the velocity in the direction of the primary motion.

The Coriolis force will induce a particle vibration along the y-axis, indicated as the secondary motion of the gyroscope or sense mode. A measurement of its amplitude allows estimating the angular velocity of the reference frame. The Coriolis acceleration is proportional to the primary motion, thus, the amplitude and the frequency of the drive oscillation have to be as large as possible. At the same time, it has to be ensured that the frequency and the amplitude remain constant; the amplitude control is accomplished by an automatic gain control loop while frequency stability is obtained by a phase locked loop.

The angular rate of the frame can be also measured by means of a closed-loop control over the secondary motion. The measurement is used to generate a control force able to annul the motion along y-axis; the control force magnitude represents the measure of the rotation rate.

2.3.1 MEMS gyro configurations

A large number of vibrating gyroscopes has been proposed whose configurations are rather complicated. They can be broadly classified with reference to the structure as follows [26]: a) vibrating beams (prismatic, triangular); b) tuning forks (single, dual, multi-tine); c) vibrating shells (hemispherical, ring, cylinder); d) vibrating plates (linear disk, angular disk, linear plate).

Vibrating shells with hemispherical and cylinder configurations are macro-sized devices while vibrating beam, tuning fork, ring and plate gyroscopes are micro-sized devices manufactured from silicon or quartz.

a) An example of a simple oscillator is reported in Fig. 11.

The sensing element is an equilateral prism, a flexural vibration is induced by piezoelectric or electrostatic elements placed at opposite sites of the prism. A periodic voltage applied to a piezoelectric actuator placed on the bottom face (A) of the beam induces a vibration along x-axis; this is the primary motion of the gyro.

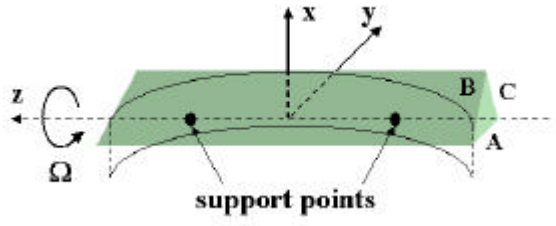

Fig. 11. Beam gyroscope structure

When the device is rotated about the longitudinal axis z, Coriolis forces produce a secondary motion, that is a vibration along y-axis. Both primary and secondary vibration, are detected by sensors placed on the two other faces (B and C) of the prism. The primary motion is sensed by summing the voltages from the two elements while the voltage contributions due to the secondary motion are opposite in phase, thus a difference is taken as measure of the angular rate. In this configuration the secondary motion is uncontrolled and its response could be sensitive to errors in cross-sectional structure, due to fabrication process, and to variable damping forces arising from the material and/or the adhesive bond.

b) The basic structure of a tuning fork vibratory gyroscope in double configuration is illustrated in Fig. 12.

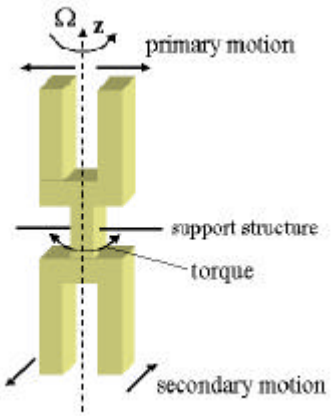

Fig. 12. Basic structure of a tuning fork vibratory gyroscope in double configuration

The tuning fork consists of two tines that are connected together via a central block attached to a supporting structure. The two upper tines are subjected to a vibration of fixed amplitude in the plane of the device. This represents the primary motion of the gyroscope. The tines vibrate in antiphase

condition so that no force results on the supporting structure from the primary motion. The actuation mechanisms used to induce primary vibration can be electrostatic, piezoresistive or piezoelectric; actuators are placed on the sides of the two tines. When the device is rotated about an axis parallel to the central axis of the fork, the primary motion generates two opposite Coriolis forces that will be able to torque the central block. In turn, the two-bottom tines experience a vibration, one opposite to the other, that is perpendicular to the direction of the primary vibration.

To detect the Coriolis-induced vibration (secondary motion), capacitive, piezoresistive or piezoelectric detection mechanisms can be used. The voltage detected by the sensors is taken as a measure of the applied rotation rate. The main advantages of a tuning fork are the stable centre of gravity and the compensation of all forces and moments of inertia in the chip.

c) A shell resonator gyroscope is based on the concept that the nodes on the circumference of a vibrating cylinder (ring) do not stay fixed with respect to the cylinder itself when it is rotated around its central axis, but they move by a quantity proportional to the turn, as sketched in Fig. 13. This is due to the Coriolis coupling between the two vibration modes that change as cos2θ (primary) and sen2θ (secondary) around the circumference.

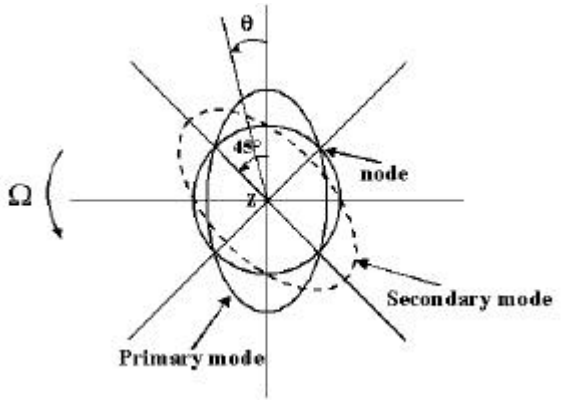

Fig. 13. Cylinder gyroscope operating principle

A certain number of electrodes are located around the circumference with the aim to excite and detect both the primary and secondary vibration modes. As an example, in Fig. 14 is illustrated a structure using eight electrodes: the pairs (1,5) and (3,7) control the primary mode while (4,8) and (2,6) detect the secondary mode. If there is no rotation the electrodes (4,8) and (2,6) check the position of nodes and there is no output. When the cylinder rotates the nodes move due to the secondary mode and the electrodes (4,8) give an output voltage.

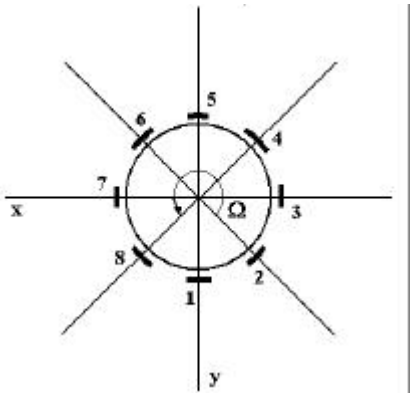

Fig. 14. Vibrating cylinder gyroscope structure using eight electrodes

The value of the output signal is used as feedback signal to the electrodes (2,6) which apply the electrical voltages to control the node position; when the output from electrodes (4,8) is zero, the voltage applied to the electrodes (2,6) is assumed as measure of the rate.

d) An example of vibratory plates gyroscope is illustrated in Fig. 15.

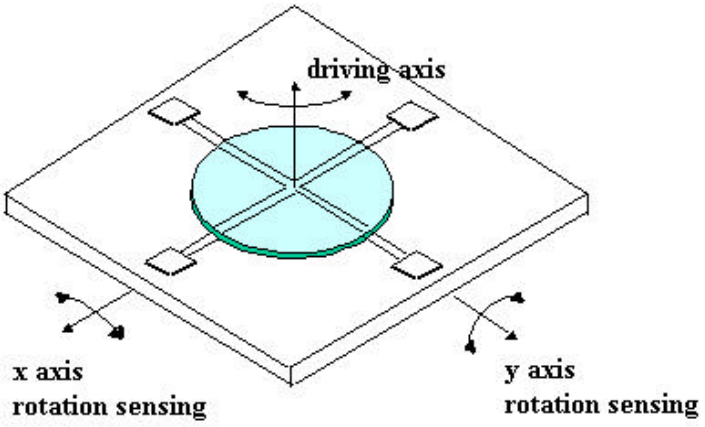

Fig. 15. Vibrating angular disk gyro structure

It is based on an angular resonance of a rigid polysilicon rotor suspended by four torsional springs anchored to the substrate. The inertial rotor is driven at angular resonance about the z-axis perpendicular to the substrate using electrostatic comb drive. A rotation rate around the x-axis induces a Coriolis angular oscillation around the y-axis and likewise a rotation rate around the y-axis induces a Coriolis angular oscillation around the x-axis. This Coriolis oscillation is usually measured using the change in capacitance between the rotor and four "quarter circle" electrodes beneath the inertial rotor. Dual axes operation can be achieved by using a different voltage modulation frequency for each pair of

diametrically placed electrodes. In this way, a rotation of the rotor in the sense axis of these electrodes generates a voltage on an integrator electrically connected to the rotor. Separate demodulation circuitry for each sense axis provides two voltage outputs proportional to angular rate inputs about respective axes.

Micromachined gyroscopes had experienced a large development because their batch processing is highly compatible with silicon IC fabrication technology. Both bulk etching of single crystal silicon and polysilicon surface micro-machining put some conditions on the geometrical structure of the device. The configuration has also to guarantee dynamic balance, decoupling and tuning of primary and secondary motions. Several devices both in silicon and piezoelectric material have been reported; they differ in structure, control and sensing. Some examples are here reported.

A bulk-micromachined, silicon MEMS vibratory gyroscope for space applications, such as altitude and maneuver control, inertial navigation system and instrumentation., has been reported [27-28]. The gyroscope has a scale factor of $(24\text{mV}/^\circ)/\text{s}$, a bias stability of 70°/h and an angle random walk of $6.3^\circ/\sqrt{\text{h}}$. A surface-micromachined x-axis vibratory gyroscope was proposed in recent years [29-30]. The sensor element is an inner wheel while the outer rectangular structure is the secondary oscillator; the device is driven by comb actuators. The gyroscope realizes the decoupling of driving and sensing mechanisms. The main performance are: resolution of 0.005 °/s, angle random walk of $0.27^\circ/\sqrt{\text{h}}$, bandwidth of 50 Hz, sensitivity of 10mV/(°/s). A vibrating ring gyroscope, fabricated through the high aspect ratio [1]combined poly and single-crystal MEMS technology (HARPSS), has been fabricated [31]. The operating principle is the same one described in section 1.3 for vibrating cylinder gyroscope. The gyroscope demonstrated a resolution of 0.5°/s in a 25 Hz bandwidth limited by the electronic noise and a zero bias drift less than 10°/s over the temperature range -40 to 85°C. By using a high aspect–ratio fabrication process a new tactical-grade device with a projected random walk as small as $0.05^\circ/\sqrt{\text{h}}$, an open-loop sensitivity of 200μV/°/s in a dynamic range of ± 250°/s was also proposed [32-33]. A micromachined single-crystalline silicon ring gyroscope with resolution of 0.005°/s, bandwidth of 70 Hz and noise floor less than 0.5°/s in 65 Hz bandwidth has been alos reported [34]. Main applications are terrestrial navigation and GPS dead-reckoning. An example of high performance vibrating shell gyro, which has found applications in spacecraft inertial reference units (IRUs), and in commercial aviation [35] is the hemispherical resonator gyro (HRG) The gyroscope has shown a bias of 1 °/hr, a random walk of 0.01 °/ hr and a scale factor ranging in 50-100

ppm and could be applied in space INS for future missions. A commercial device in quartz by Litton is also available claiming a bias stability of 0.003 °/ hr.

A vibrating quartz gyros in double tuning fork configuration is reported [36]. The same technology is used for the gyro used in an Inertial Measurement Unit also in production. For this device a resolution less than 0.002 °/s in a bandwidth of 60 Hz and temperature range of - 40 to 80 °C is reported. The full range is ± 100 °/s and the output noise is 0.01 $°/s/\sqrt{Hz}$. This gyroscope finds application in automotive, commercial aircraft, helicopter, marine systems, tactical missiles, military aircraft. Further possible applications are onboard of spacecraft for antenna stabilization, flight event initiation, instrumentation, maneuvering system, spin monitoring, stability and control.

From what described in this subsection it appears clear that the existing devices are mainly used for non-space applications or for applications in space in which inertial grade performance is not required. However, vibrating gyros seem to be useful for inertial systems.

2.3.2 Open issues and design criteria

As it was already explained, vibratory gyroscopes can work in open or closed loop mode to measure the angular velocity. If there is a change in the rotation rate, the amplitude of the sense mode doesn't change instantaneously but it required some time to reach the steady state. With matched sense and drive resonant modes, the time response, approximately equal to $2Q/\omega$, where Q is the mechanical quality factor, limits the bandwidth of the sensor to a few hertz. The bandwidth of gyroscope operating in an open-loop mode can be increased with a slight mismatch in the sense and drive mode resonant frequencies but, at the same time, this reduces the sensitivity. In the closed-loop-operating mode, the amplitude of sense mode is continuously monitored and set to zero; this means that the bandwidth and the dynamic range of the sensor can be greater than the corresponding open-loop values even with matched resonant modes. The bandwidth is then limited by the readout and control electronics and can be increased to values approaching the resonant frequency of the structure.

For a gyroscope rotating around z-axis and driven in the x direction, sensitivity can be expressed by:

$$\Delta y = 2\Omega \frac{F_e}{m\omega_x} \frac{1}{\sqrt{\left(\frac{\omega_y}{Q_y}\right)^2 \omega_x^2 + \left(\omega_x^2 - \omega_y^2\right)^2}} \qquad (10)$$

[1] Aspect ratio is the ratio of the height of the grown structure over the lattice constant.

where Δy is the displacement due to the Coriolis acceleration, F_e is the driving force, m the inertial mass, Q_x, Q_y, ω_x and ω_y the mechanical quality factor and the resonant frequency in the driving and the sensing mode, respectively.

The gyroscope resolution depends on different parameters. In open loop mode with matched sense and drive resonant modes, the resolution can be improved by reducing the noise of the readout circuit, increasing the Coriolis-induced capacitance change of the device, lowering the resonant frequency, increasing the mechanical quality factor and minimizing the parasitic capacitances. Even if a lower resonant frequency of the structure can improve the sensitivity, it must be greater than the environmental noise (> 2 kHz) to get better signal. Stronger Coriolis forces will be obtained by increasing the amplitude of vibration in the drive mode. If the proof mass oscillates in vacuum, very high quality factor can be obtained. Q can be strongly increased by significantly reducing energy losses and it can be got if the resonant structure operates in vacuum. This requires hermetically sealed, robust vacuum-packaging techniques, such us those using silicon or glass wafers bonded to the sensor substrate.

Furthermore, if the resonant frequencies of drive and sense modes are matched, Q amplifies the coupling and the resolution is then increased. The difficulty is to design the device in a way such as the two resonance frequencies are perfectly matched (better than 1 Hz) over the temperature range and other environmental factors. The tolerances in the fabrication process are very high to control; thus normally an active tuning is used.

An important performance parameter for a vibratory gyroscope is its zero rate output (or zero bias). Imperfections in the geometry of the vibrating mechanical structure, in the electrodes that control the sense and drive modes or in the electrical coupling between these electrodes, asymmetric damping of the structure can produce an output signal even in the absence of rotation. This error, called the quadrature error, can be sometime orders of magnitude larger than Coriolis signal, and, of course, it may cause errors in sensing the rotation rate. ZRO can be significantly reduced by electrically and mechanically decoupling the sense and drive modes and by reducing the fabrication process errors. Moreover, high-quality materials with low internal damping will also reduce the ZRO and, in any case, any residual zero bias error should then be further reduced electronically.

A high-performance gyroscope should have an accurate scale factor, with small temperature sensitivity, on a wide dynamic range, about 140 dB. To obtain good results a particular attention has to be paid to the materials, which form the structure. Using several materials in the same structure can

cause changes of scale factor with the temperature; best performance can be obtained in all-silicon devices. Temperature changes can induce variation of the resonant frequency and this can, in turn, affect the scale factor; some compensation in temperature of the scale factor could be required.

Another concern about a vibrating mechanical element is the long-term drift and fatigues problem, then the reliability of the device. Low-noise electronics for readout, processing and control is necessary for operation both in open and closed loop mode. Monolithic integration of the sensor and the readout electronics reduces the parasitic effects and improves the resolution of the sensor.

2.4 Micro-optical-electromechanical systems (MOEMS) gyros

Optical MEMS sensors have been under development since several years. The aim is to increase the accuracy of micro-inertial sensors for highly precise navigation. It is quite difficult to design a micro-optical gyroscope because their small dimensions prevent them having a path large enough to detect low rotation rates. Design techniques for MOEMS devices can be found in [37].

An interferometric MOEMS gyroscope (MIG) has been proposed by Air Force Institute of Technology (AFIT) [38], as in Fig. 16. In this open loop device, the basic concept of the interferometric fiber optic gyroscope is integrated with MEMS. The MEMS mirrors are placed on a silicon substrate to create a spiral path for the light from the outside, where the laser is placed, to the center of the die, where the interference pattern is detected. The mirrors are arranged in such a way to increase the path length of the device with respect to a standard Sagnac interferometer. The propagation is in free-space and the laser beam only interacts with mirrors on the corners of the spiral path to keep the losses low.

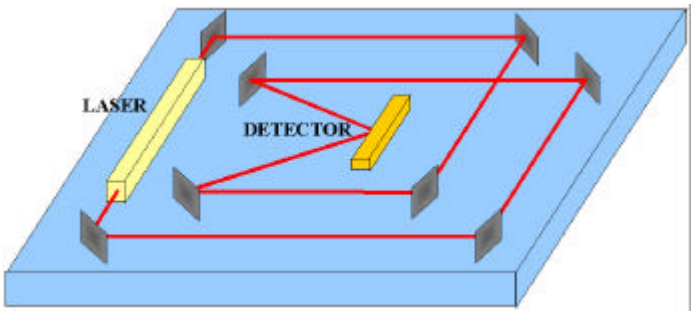

Fig. 16. Scheme of MIG approach

The difference of the AFIT – MIG with respect to the standard Sagnac interferometer is that the previous one is not a circular but a spiral design. Its operation is based only on the total path length and not on the geometry of the path. Each part of the path is considered and the related time difference is determined. The sum of the different results is independent of the path geometry and it is converted to a phase difference.

The fundamental limit of detection associated with such a kind of device is due to photon shot noise, that is an uncertainty in the current generated at the detector, corresponding to the intensity of the interfering beams. This intensity is a function of the phase difference due to the rotation. The fundamental limit of detection is a measure of the minimum change in the detectable rotation rate. When the noise level is too high the interferometer will not be able to sense any rotation rate.

The detection limit is function of the path length of the interferometer: for a nine-leg interferometer the parameter is 0.0118 rad/sec or 0.6761°/sec. As the number of the optical legs increases, the detection limit decreases: it is reduces by a factor of almost 2 when the optical legs is doubled. This parameter value is useful for both military and civilian applications. Furthermore, the detection limit is also function of the quality of laser and detector used, and then high quality detector must be used to determine small rotation rate. For the above considerations small devices have difficulty achieving reasonable performance. Then, it should be used in civilian and military applications.

A hybrid MOEMS gyroscope has been also proposed [39]. It consists in a MEMS resonator to sense the inertial Coriolis force and an optical readout performed by a laser diode that acts as an injection interferometer. The laser beam impinges the resonating structure; the retroreflection is injected back into the laser source and this generates amplitude modulation of the laser power. The gyroscope has an angle random walk of $(0.6°/\mathrm{h})/\sqrt{\mathrm{Hz}}$ as a first result.

2.5 Future trends and conclusions

The current major obstacle to a larger use of Inertial Navigation System (INS) is the system stability and high cost. High performance sensors are required to improve INS technology, together with advances in computer technology (memory and throughput), power quality, and electronics.

For high performance space applications, reduction of power, size and weight, by improving the integration of optical functions external to the fibre loop, and drift stability, by using closed-loop configurations with integrated phase modulation block, are required to IFOGs.

The main issue for active ring resonator gyros is the reduction of the lock-in effect that requires design and technology efforts such as the reduction of backscattering centres inside the active structure, together with a strong reduction of size for integrated solution. Good perspectives appear for performance of passive ring resonator gyros: the use of silicon technology will allow reducing optical losses, then quantum limit, and radius, then size.

Continuous improvement of the performance is required for MEMS gyros. This means a particular care in material uniformity, mixed micromachining fabrication processes on silicon and deep etching techniques allowing high quality factor of the structures, robust vacuum packaging techniques and tuning in frequency to compensate sensor drifts and long-term effects. Low- noise and low-drift interface electronic circuitry is also required. A strong integration effort will allow to implement devices for inertial platforms, fabricating multiaxis devices on a single chip together with accelerometers and electronics. Further issues are cost and reliability.

At near term, MEMS and improved fiber optic technology are expected to replace RLGs and mechanical devices while RLGs are superior over IFOGs when high scale factor stability is required. Mechanical gyros and accelerometers are still expected to be used in guidance systems. IFOGs and MEMS/MOEMS are used for guiding re-entry bodies.

At far term, MEMS and integrated optics gyros will dominate the low and medium performance range due to orders of magnitude in performance improvement, design improvement and higher level of integration. Integrated optics gyro are expected to be used when navigation grade is required since MEMS show some restrictions. Moreover, integrated optics gyros would be no "g" sensitive devices. IFOGs should become dominant for strategic application.

References

[1] N. Barbour, G. Schmidt, "Inertial Sensor Technology Trends", *IEEE Sensors Journal*, vol. **1**, n. 4, pp. 332-339, 2001.

[2] M.N. Armenise, C. Ciminelli, F. De Leonardis, R. Diana, F. Peluso, V.M.N. Passaro, "Micro Gyroscope Technologies for Space Applications", *Internal Report, ESA-ESTEC IOLG PROJECT*, Contract DEE-MI, May 2003.

[3] I. A. Andronova, G. B. Malykin, "Physical problems of fiber giroscope based on the Sagnac effect", *Physics-Uspekhi* vol. 45, n. 8, pp. 793-817, 2002.

[4] M. Komachia, H. Sonobe, S. Oho, K. Ohbu, T. Yuhara, H. Izuka, "Secondary- phase modulation method for open loop fiber optic gyroscopes", *Applied Optics*, vol. 35, no. 19, pp. 3719-3725, July 1996.

[5] R. A. Bergh, H. C. Lefevre, H. J. Shaw, "An Overview of Fiber-Optic Gyroscopes", J. Lightwave Technol., vol. 2, n.2, pp. 91-107, Feb. 1984.

[6] H. C. Lefevre, P. Marten, J. Morrise, P. Simonpieti, P. Vivenot and H. J. Arditty, "High dynamic range fiber gyro with all digital signal processing", in *Fiber Optic and Laser Sensors.*

[7] http://www.lmcontrolsystems.com/FactSheets/RRGU.pdf

[8] http://www.ngnavsys.com

[9] G. A. Pavlath, "Fiber optic gyro based inertial navigation systems at Northrop Grumman", *Optical Fiber Sensors Conf. Tech. Dig.*, OFS 2002, vol. 1, p. 9.

[10] http://www.kvh.com

[11] R. B. Dyott, S.M. Bennett, D. Allen, J. Brunner, "Development and Commercialization of Open Loop Fiber Gyros at KVH Industries", *IEEE Optical Fiber Sensors Conf.*, 15th OFS 2002, pp. 19 -22.

[12] J. P. Jilmore, L. Freier, E. Nolan, M. Perlmutter, M. Bowser, J. Maglieri, "Three-Axis Nested Fiber Optic Gyroscope", http://www.fibersense.com.

[13] IFOG by Optolink Ltd., Moscow Institute of Electronic Technology, http://www.miee.ru/english/e1.html

[14] http://www.astrium-space.com

[15] M. Dollon, G. Cros, A. Sevellec, P. Antoine, G. Muller, E. Willemenot, A. Urgell, G. Hardy, T. Loret, N. Faussot, Y. Cottreau, T. Gaiffe, "A new family of IMU based on IFOG technology", *Proc. V ESA Conf. On Spacecraft Guidance, Navigation and Control, Frascati, Italy*, 22-25 Oct 2002, SP-516, pp. 41-45.

[16] S. J. Sanders, L. K. Strandjord, D. Mead, "Fiber optic gyro technology trends - a Honeywell perspective", *Optical Fiber Sensors Conf. Tech. Dig., OFS 2002*, vol. 1, pp. 5-8.

[17] W. W. Chow, J. Gea-Banacloche, L. M. Pedrotti, V. E. Sanders, W. Schleich, M. O. Scully, "The ring laser gyro", *Rev. of Modern Optics*, vol. **57**, n.1, pp. 61-104, 1985.

[18] H. Haus, H. Tatz, W. Smith, "Frequency Locking of Modes in a Ring Laser", *IEEE J. Quantum Electron.*, vol. **QE-21**, no. 1, pp. 78-85, Jan 1985.

[19] http://www.ais.honeywell.com/dss/sgp/products/rlg-gg1305an.htm

[20] http://www.ngnavsys.com/Html/LN-100LG/

[21] http://www.aselsan.com.tr/mging/products/ln100.htm

[22] European Patent EP 1219926 "Integrated optical angular velocity *sensor*", by *M.N. Armenise, M. Armenise, V.M.N. Passaro, F. De Leonardis, Politecnico di Bari*, filed on 28.11.2000.

[23] M.N. Armenise, V.M.N. Passaro, F. De Leonardis, M. Armenise, "Modeling and Design of a Novel Miniaturized Integrated Optical Sensor for Gyroscope Applications", *J. Lightwave Technology*, vol. **19**, n. 10, pp. 1476-1494, 2001.

[24] C. Monovoukas, A.K. Swiecki, F. Maseeh, "Integrated optical gyroscopes offering low cost, small size and vibration immunity", *Intellisense Corp. Report*, 2000, http://www.intellisense.com/contentfiles/devicetechnologypapers/IntegratedOpticalGyroscopesofferinglowcostsmallsizeandvibrationimmunity.pdf

[25] K. Suzuki, K. Takiguchi, K. Hotate, "Monolithically Integrated Resonator Microoptic Gyro on Silica Planar Lightwave Circuit", *J. Lightwave Technology*, vol. **18**, n. 1, pp. 66-72, 2000.

[26] L. O. Thielman, S. Bennett, C.H. Barker, M. E. Ash, "Proposed IEEE Coriolis Vibratory Gyro Standard and Other Inertial Sensor Standards", *IEEE Position Location and Navigation Symp.*, 2002, pp. 351-358.

[27] T. K. Tang, R. C. Gutierrez, J. Z. Wilcox, C. Stell, V. Vorperian, R. Calvet, W. J Li, I. Charkaborty, R. Bartman, W. J. Kaiser: "Silicon bulk micromachined vibratory gyroscope", *Tech. Dig. Solid-State Sensor and Actuator Workshop,* Hilton Head Island, SC, Jun 1996, pp. 288–293.

[28] T. K. Tang, R. C. Gutierrez, C. B. Stell, V. Vorperian, G. A. Arakaki, J. T. Rice, W. J. Li, I. Chakraborty, K. Shcheglov, J. Z. Wilcox, W. J. Kaiser: "A packaged silicon MEMS vibratory gyroscope for microspacecraft", *Proc. IEEE Micro Electro Mechanical Systems Workshop (MEMS'97),* Japan, 1997, pp. 500–505.

[29] W. Geiger, B. Folkmer, J. Merz, H. Sandmaier, W. Lang: "A new silicon rate gyroscope", *Proc. the 11th IEEE Micro Electro Mechanical Systems Workshop (MEMS'98),* Heidelberg, Germany, Feb 1998, pp. 615–620.

[30] W. Geiger, W. U. Butt, A. Gaiâer, J. French, M. Braxmaier, T. Link, A. Kohne, P. Nommensen, H. Sandmaier, W. Lang, H. Sandmaier: "Decoupled microgyros and the design DAVED", *Sensors and Actuators A,* vol. **95**, pp. 239–249, 2002.

[31] M. W. Putty, K. Najafi: "A micromachined vibrating ring gyroscope", *Tech. Dig. Solid-State Sensor and Actuator Workshop,* Hilton Head Island, SC, Jun 1994, pp. 213–220.

[32] F. Ayazi, K. Najafi: "Design and fabrication of a high performance polysilicon vibrating ring gyroscope", *Proc. the 11th IEEE Micro Electro Mechanical Systems Workshop (MEMS'98),* Heidelberg, Germany, Feb 1998, pp. 621–626.

[33] F. Ayazi, K. Najafi: "A HARPSS Polysilicon Vibrating Ring Gyroscope", *IEEE J. of Microelectromech. Syst.*, vol. **10**, no. 2, p. 169-179, Jun 2001.

[34] I. Hopkin: "Performance and design of a silicon micromachined gyro", *Proc. Symp. Gyro Technology*, Stuttgart, Germany, 1997, pp. 1.0–1.10.

[35] J. Dickinson, C. R. Strandt, **"**HRG strapdown navigator**",** *IEEE Position Location and Navigation Symp. 'The 1990's - A Decade of Excellence in the Navigation Sciences'*, IEEE PLANS '90, 20-23 Mar 1990, pp. 110 –117.

[36] "BEI GYROCHIP™ Model QRS11 data -sheet": http://www.systron.com/PRODINFO/QRS11.html

[37] J. R. Gilbert, **"**Exploring design spaces for optical MEMS devices", *Advanced Applications of Lasers in Materials Processing, 1996/Broadband Optical Networks/Smart Pixels/Optical MEMS and Their Applications*, IEEE/LEOS 1996 Summer Top. Meet., 5-9 Aug 1996, pp. 54 –55.

[38] J. Stringer, "The Air Force Institute of Technology (AFIT) Micro Electro-Mechanical Systems (MEMS) Interferometric Gyroscope (MiG)", *Thesis presented to the Faculty of the Graduate School of Engineering and Management*, Mar 2000.

[39] M. Norgia, S. Donati: "Hybrid opto-mechanical gyroscope with injection-interferometer readout", *Electron. Lett.*, vol. **37**, no. 121, pp. 756-758, Jun 2001.